Chemical Science

ROYAL SOCIETY OF CHEMISTRY

EDGE ARTICLE

View Article Online
View Journal | View Issue

Cite this: *Chem. Sci.*, 2025, **16**, 17850

All publication charges for this article have been paid for by the Royal Society of Chemistry

Regulating enol–keto tautomerism at the single-molecule level with a confined optical field

Adila Adijiang,†[a] Yunlong Ge,†[b] Hefa Feng,[a] Yan Yan,[b] Xin Zuo,[a] Haoyu Wang,[a] Xueyan Zhao,[ac] Min Tan,[ad] Surong Zhang,[a] Xiaona Xu,[ae] Lichuan Chen,[a] Chuankui Wang,[b] Zongliang Li *[b] and Dong Xiang *[a]

Received 11th August 2025
Accepted 26th August 2025

DOI: 10.1039/d5sc06085k

rsc.li/chemical-science

The keto–enol tautomerism, involving a reversible isomerization of the molecule, plays a critical role in organic synthesis, biological activity, and molecular-scale charge transport. It is therefore essential to manipulate the process of keto–enol tautomerism. Unlike typical ketones, β-diketones exist dominantly in the enol form and it is a great challenge to realize enol–keto tautomerism due to the formation of intramolecular hydrogen bonds in the enol form. Here, *via in situ* monitoring of the conductance evolution of thousands of single-molecule junctions, we demonstrated that the enol → keto transformation can be significantly promoted by confined ultraviolet (UV) irradiation at an extremely low intensity (1‰ of sunshine) employing antenna electrodes. Our study reveals that the conductance of the enol form is an order of magnitude larger than that of the keto form although both have similar molecular lengths and identical anchoring groups, and the enol form shows a current rectification behaviour which is completely absent in the keto form. Supported by UV-vis measurements, wavelength-dependent conductance measurements, and theoretical calculations, the mechanism for the enol → keto transformation promoted by the gap-electrode-confined optical field was elucidated, offering a new strategy to regulate the tautomerism processes at the single molecule level, and implying a potential multi-functional application of β-diketones in the fabrication of rectifiers and synchronous switches.

Introduction

Keto–enol tautomerism has played an important role in the fields of organic synthesis, pharmacy, photocatalysis, and biomarker detection.[1–6] Typically, the process of keto–enol tautomerism can be promoted or controlled by chemical modulation, *e.g.*, catalytic agents and pH value,[7,8] or by redox control.[9] However, the chemical modulations are limited for wide application since the addition of chemical components might change the chemical/physiological environment and damage the target molecular functions, and thus a physical modulation strategy, such as light irradiation, is highly desired. However, the modulation of tautomerism by light at the individual level, to the best of our knowledge, is rarely reported, mainly because (1) the energy supplied by a normal light source cannot overcome the energy barrier for tautomerism,[10] and the change of wavelength to achieve high energy typically leads to side effects; and (2) the field distribution of a typical light source is uniform and it is difficult to confine the light energy into a molecule-scale space;[11] thus it is great challenge to regulate the enol–keto tautomerism by light at the single molecule level. Therefore, it is important to find a class of molecules and an appropriate light incident strategy to trigger the tautomerism processes with normal or low-power light irradiation. Unlike general ketones, β-diketones exhibit a much higher proportion of the enol form, which is attributed to the stabilizing effect of intramolecular hydrogen bonds.[1,8] Non-covalent hydrogen bonds can be cleaved by photon-absorption-enhanced vibration,[12] which makes β-diketones a promising candidate to be regulated by light irradiation.

In this study, we explore the *in situ* conductance evolution of β-diketone derivatives upon UV irradiation employing the scanning tunnelling microscopy break-junction (STM-BJ) technique,[13–15] in which a nanocavity and localized surface plasmon (LSP) are generated between two electrodes upon light irradiation.[11,16] LSP can confine the optical field to dimensions

[a]*Tianjin Key Laboratory of Micro-scale Optical Information Science and Technology, Institute of Modern Optics and Centre of Single-Molecule Science, Nankai University, Tianjin 300350, China. E-mail: xiangdongde@126.com*

[b]*Key Laboratory of Medical Physics and Image Processing of Shandong Province, School of Physics and Electronics, Shandong Normal University, Jinan 250358, China. E-mail: lizongliang@sdnu.edu.cn*

[c]*School of Physics and Electronic Engineering, Northeast Petroleum University, Daqing, China*

[d]*College of Optical and Electronic Technology, China Jiliang University, Hangzhou 310018, China*

[e]*Department of Chemistry, Tsinghua University, Beijing 100084, China*

† These authors contributed equally.

much smaller than the free-space optical wavelength, breaking the limitation of optical diffraction.[11] Our experimental and theoretical study demonstrated that the transformation of β-diketone from the enol to keto form inside the nanocavity can be greatly promoted by p-polarized UV illumination with a low power density (three orders of magnitude smaller than that of solar power[17]) due to the enhanced light field exerted on the photo-excited β-diketone which breaks the intramolecular hydrogen bonds and thus promotes the enol to keto transformation.

We found that the conductance of β-diketone in the enol form is an order of magnitude higher than that of the keto form, which can mainly be attributed to the hydrogen bond in the enol form providing an additional charge transport channel in the molecular junction, thus greatly facilitating the charge transport through the molecule junctions.[18–20] This result implies that, on one hand, conductance measurements can be used to distinguish the tautomer at the single-molecule level, enabling detection at extremely low concentrations.[21] On the other hand, the disparate conductance indicates that single-molecule conductance switches can potentially be fabricated based on the keto–enol tautomer *via* UV stimulation,[9,22] which is a great challenge for most photochromic molecules due to the quenching of the excited state of the molecules in the presence of the Au electrodes.[23–25] In addition to the UV-modulated switching behaviour, the enol form shows rectification behaviour which disappears after the transformation to the ketone form, implying a potential multi-functional application in rectifiers and synchronous switches.

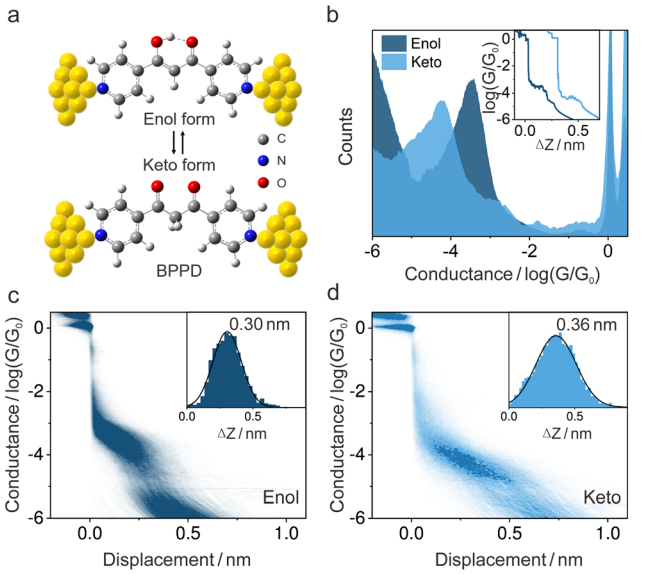

Fig. 1 Conductance of BPPD single-molecule junctions in two kinds of solvents with two favourable forms. (a) Schematic of single-molecule junctions in the enol and keto form. (b) Conductance histograms of BPPD junctions with the favourable enol (green) and keto form (blue) measured in TCB and water. (Inset) Typical conductance–displacement traces of BPPD in two solvents. (c and d) Two-dimensional conductance histograms of BPPD molecular junctions with the favourable (c) enol form and (d) keto form. (Insets) The distributions of relative stretching distances of the single-molecule junctions in TCB and water.

Results and discussion

Determining the conductance of single molecules in two forms

β-Diketone derivative 1,3-bis(pyridine-4-yl) propane-1,3-dione (denoted as BPPD) with pyridine anchoring groups at both ends was selected as the target molecule. Conductance measurements were conducted using the STM-BJ technique in solution with gold electrodes, see the Method section for details. Fig. 1a schematically illustrates the configurations of BPPD in enol and keto forms. In the enol form, a stable six-membered ring (chelate ring) within the molecular skeleton is formed *via* an intramolecular hydrogen bond, which is the predominant form in non-polar solvents.[1] In contrast, the keto form is favoured in protic solvents due to the fact that the hydrogen bond donor and acceptor groups of the BPPD molecule can form intermolecular hydrogen bonds with solvent molecules,[20,26,27] which shifts the equilibrium towards the keto form.

To demonstrate that the enol → keto transformation can be promoted by light illumination in the nanocavity, we first measured the conductance of BPPD in 1,2,4-trichlorobenzene (TCB, a non-polar solvent) which favours the enol configuration and in water (protic solvent) which prefers the keto configuration.[26] Fig. 1b presents the 1D conductance histograms for BPPD in the two solvents, and each histogram was built from approximately 3000 traces without data selection, revealing a significantly higher conductance in TCB ($10^{-3.47}$ G_0) compared to that in water ($10^{-4.25}$ G_0). Here, G_0 is the quantum of conductance, ~77.5 μS. Fig. 1c and d show two-dimensional (2D) conductance histograms of BPPD in TCB and water. The insets of Fig. 1c and d show the probable length of the conductance plateau. Adding 0.5 nm for the snap-back distance of gold atoms,[28,29] we obtain conductance plateaus of 0.80 nm and 0.86 nm in the two solvents, which is consistent with the molecular length in the enol and keto form. In contrast, these evident peaks are completely absent in the histograms when the experiments are performed in pure solvent without BPPD, see SI S1 for details.

To confirm that BPPD adopts different configurations in TCB and water, we performed ultraviolet-visible (UV-vis) spectroscopy measurements in the two solvents, as depicted in Fig. S4. The UV-vis spectrum of BPPD in TCB, reveals an enol-type peak at 341 nm, confirming the presence of the enol form of BPPD in TCB.[30] In contrast, an absorption peak at 265 nm is observed in water, indicating the keto form's predominance.[30] The measured UV-vis spectrum confirms that BPPD adopts the dominant enol form in TCB but the keto form in water.

Compared with the keto form, the much higher conductance of BPPD in the enol form can be attributed to three factors: (i) the enol form's molecular skeleton, featuring carbon–carbon double bonds in the middle of the molecule, enhances conjugation and aromaticity compared to the keto form's σ bridge, thereby enhancing the conductance.[31] (ii) Intramolecular

hydrogen bonds in the enol form act as non-covalent conformational locks, aligning the two terminal pyridine rings in the same plane and thus promoting the planarization of the molecules.[32–34] A smaller the dihedral angle between the two benzene rings leads to a higher degree of conjugation and thus higher conductance.[31,35] (iii) Intramolecular hydrogen bonds offer an additional pathway for charge transport, enhancing the conductance of the enol form molecular junctions.

Flicker noise and current–voltage characterization

It is well established that the feature of flicker noise reflects the electronic coupling state between molecule and electrode[36] and can be employed to diagnose the charge transport pathway.[14,37,38] The flicker noise power (PSD) shows a power–law dependence on the junction average conductance (G), PSD $\propto G^n$, where the scaling exponent n is used as an indication for the coupling type: n close to 1.0 indicates through-bond coupling; n close to 2.0 indicates through-space coupling.[36] For PSD characterization, we suspended the tip for 150 ms during the tip retraction process when the molecular junction was formed. More than 10 000 conductance–time (G–t) traces under a fixed bias voltage were collected and used to build the PSD. The typical G–t traces recorded during the suspension period are shown in Fig. 2a. Analysis of the PSD revealed that the noise power scales as $G^{1.9}$ for BPPD-enol in TCB (Fig. 2b), suggesting the dominance of through-space transport and thus confirming that the non-covalent hydrogen bonds was truly formed. In contrast, the noise power scales as $G^{1.3}$ for BPPD-keto in water (Fig. 2c) indicative of dominant through-bond transport. The PSD features indicate that the intramolecular hydrogen bond actively participates in electron transport in the BPPD-enol form molecular junction, significantly enhancing the molecular conductance.

To further explore the role of intramolecular hydrogen bonds in charge transport, thousands of I–V curves of the molecular junctions were recorded. For this purpose, the movement of the top electrode was suspended automatically *via* a feedback system once a stable molecular junction was formed. Subsequently, the voltage sweeping mode was triggered, and the corresponding I–V curves were recorded and collected to build a two-dimensional (2D) I–V density map.[39] Fig. 2d displays the typical individual I–V curves, and Fig. 2e and f present the 2D I–V density maps of BPPD molecular junctions in enol and keto forms. Interestingly, the typical I–V curves and the 2D density map of BPPD in the enol form show obvious asymmetric characteristics (rectification feature). In contrast, the rectification behaviour almost completely disappears in the keto form. This rectification property can be attributed to the asymmetrical structure of the enol form.[40–42] The calculation of the electrostatic potential (ESP) further reveals that the ESP changes asymmetrically upon a reversed external electric field (Fig. S5), which also leads to a rectification behaviour.

The dipole moment is also a crucial parameter affecting the rectification properties of molecular junctions.[18] It has been demonstrated that the charge transport direction can be

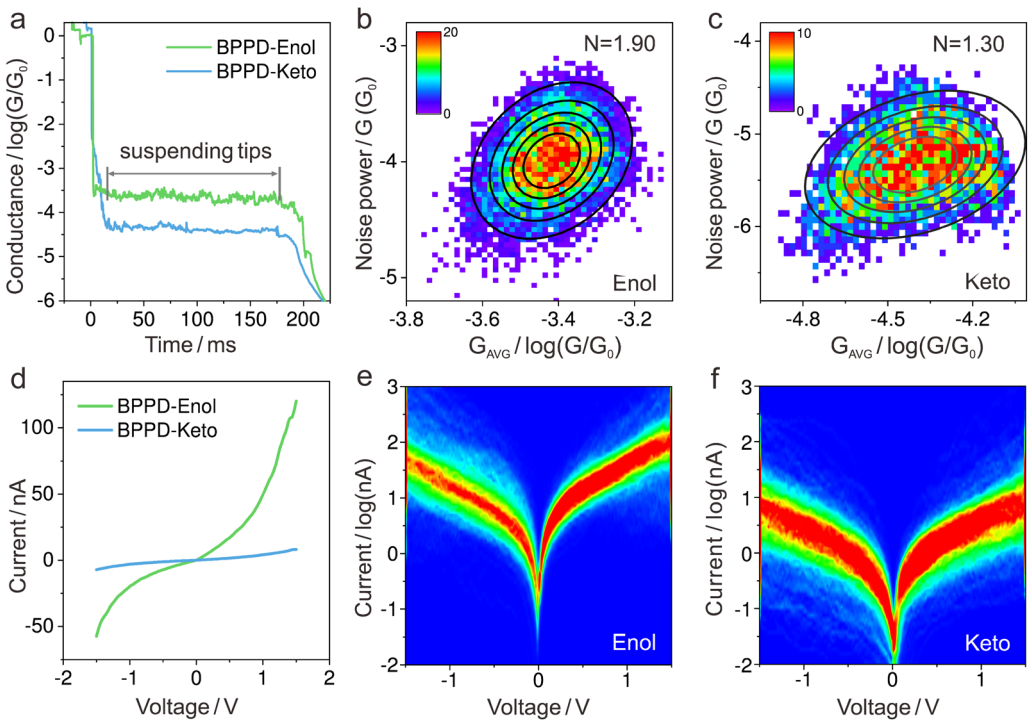

Fig. 2 Flicker noise and current–voltage characterization of BPPD molecular junctions with enol/keto forms in two solvents. (a) Typical conductance–time traces of BPPD molecular junctions recorded during the suspension process of the tip. (b and c) 2D histograms of normalized flicker noise power *versus* average conductance (G_{AVG}) of BPPD junctions with the (b) enol form in TCB and the (c) keto form in water. (d) Typical I–V curves of BPPD molecular junctions in enol and keto forms. (e and f) 2D I–V histogram for BPPD in the (e) enol form and (f) keto form.

controlled by the dipole orientation of the molecules.[40,43] The calculation of the dipole moment shows that BPPD-enol has a non-zero dipole moment and asymmetrically changes upon an external field (Table S1 and Fig. S6), which results in rectification behaviour in the single-molecule junction. Notably, the observation of the statistical rectifying behaviour of the enol form indicates that BPPD-enol has a favourable adsorption orientation with respect to the biased electrodes,[44–46] otherwise the rectifying feature would disappear in the 2D *I–V* density map, which was built with thousands of random molecular junctions. Interestingly, the enol form possesses only a trivial asymmetry in structure with respect to the electrodes, *i.e.*, the anchoring group and the molecular backbone are symmetric and only the central single hydrogen bond is spatially asymmetric with respect to the two electrodes. However, the rectification ratio can reach 2 within a small bias window, indicating that the hydrogen bond plays a critical role in determining the rectification feature.

Regulation of keto–enol tautomerism by UV irradiation

The significant conductance disparity in BPPD isomers signifies that they are promising candidates for molecular functional devices. To harness this potential, we should find ways to interconvert these configurations effectively. Since ultraviolet light, in principle, has the ability to break hydrogen bonds by enhancing vibrations,[47] we assume that UV irradiation may promote the transition of BPPD from the enol to the keto form. With this speculation, we applied *in situ* UV irradiation to BPPD in TCB. UV light with a central wavelength of 365 nm (full width at half maximum: 14.2 nm) was used as the incident light source. Notably, the power density of the incident light is quite small, ~0.01 mW cm^{-2}, which is three orders of magnitude smaller than the typical solar power density (50 mW cm^{-2}) on the Earth's surface.[17]

Fig. 3a shows schematically the molecular junctions formed in dark employing the STM-BJ technique. Fig. 3b shows the scheme of a molecular junction upon light illumination under a small incidence angle (5 ± 2°) with respect to the substrate plane and polarized parallel to the incident plane (p-polarization). A gradual shift in the conductance peak position from the BPPD-enol dominated position to the BPPD-keto dominated position was observed upon UV irradiation, as depicted in Fig. 3c. The peak in Fig. 3c at 0.0 h, signifies that the most probable conductance of BPPD-enol junctions is approximately $10^{-3.4}$ G_0 before light irradiation. The peak at 3.0 h indicates that the most probable conductance of the molecular junctions recorded during the irradiation period from 2.5 to 3.0 h is $10^{-4.2}$ G_0, which agrees well with the probable conductance of BPPD-keto measured in water as presented in Fig. 1b. Beside the main peak, a small shoulder peak with a lower conductance value can be observed in each histogram of Fig. 3c, which can be attributed to varied contact geometries of the pyridine anchoring group.[39,48] The corresponding 2D conductance histograms recorded at different irradiation periods are shown in Fig. S7, which confirm the conductance evolution trend (gradually decreases upon UV irradiation) as presented in 1D conductance histograms.

Fig. 3d shows the 2D conductance evolution *in situ* upon continuous UV irradiation, in which a gradual shift of the probable conductance can be clearly observed, *i.e.*, the conductance shifts from a TCB terminated value to a water terminated value as presented in Fig. 1. We proposed that UV irradiation with a greatly enhanced optical field inside the nanocavity breaks the intramolecular hydrogen bonds in BPPD-

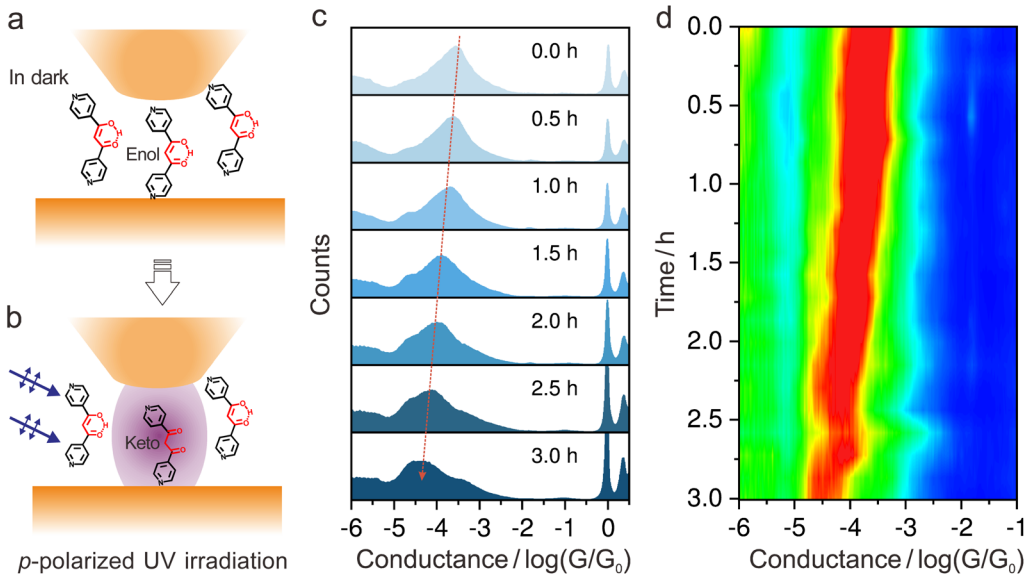

Fig. 3 Conductance evolution of BPPD-enol molecular junctions upon *in situ* UV irradiation in TCB. (a) Schematic diagram of the STM-BJ technique performed in dark in which BPPD exists in the enol form, and (b) under p-polarized laser irradiation in which BPPD-enol inside the nanogap was transformed to BPPD-keto. (c) 1D conductance histograms of BPPD-enol junctions during *in situ* UV irradiation. (d) 2D conductance evolution of BPPD-enol junctions upon UV irradiation.

enol, triggering photoisomerization between the enol and keto forms. Notably, Fig. 3d shows a small fluctuation around 2.7 h, which can be attributed to the refined interval used for data statistics. The gradual conductance shift presented in Fig. 3c and d reflects the statistical mixture of junction states. Upon UV irradiation, more molecules were transformed from the enol-form (high-conductance) to the keto-form (low-conductance). Therefore, the probable conductance determined from the conductance histogram gradually shifts to a low value. The flicker noise measurement upon UV irradiation (2.5 h–3.0 h) shows that noise power scales as $G^{1.3}$, indicating a dominant through-bond transport mechanism, the same as for BPPD-keto, see SI Fig. S8. The conductance evolution and flicker noise features signify that the enol form is gradually transformed to the keto from upon light irradiation. The hypothesis that more molecules in the enol form are transformed to the keto form was confirmed by *in situ* UV-vis measurements, see Fig. S9 for details.

To clarify whether the conductance change is due to the photoisomerization of β-diketone or originates from the excitation of the pyridine anchor group,[15] we constructed control molecular junctions with 4,4′-trimethylenedipyridine (PY-3C), which has a structure similar to BPPD with two pyridine anchor groups but without the β-diketone core group. The conductance measurements show that the probable conductance of PY-3C remains unaffected upon UV irradiation, see SI Fig. S10 for details. This control experiment suggests that the pyridine anchor groups do not play a critical role in determining the conductance evolution upon light illumination under such low-power UV (365 nm) irradiation. We further conducted a wavelength dependent experiment on BPPD-enol molecular junctions by exposing them to blue and red light (450 nm and 633 nm) with equivalent intensity to UV light, see SI Fig. S11. No change was observed in the position of the conductance peak, indicating that light irradiation with longer wavelengths does not induce isomerization of BPPD molecules.

Mechanism for promoted transformation

To clarify why the enol and keto forms show large differences in conductance, we performed calculations based on density functional theory (DFT) combined with the nonequilibrium Green's function (NEGF) method.[49–51] Considering that a gold ball fabricated by burning one end of a gold wire is used as the top electrode and a substrate with a sputtered gold layer is used as the bottom electrode in which an atomic protrusion typically exists, the two electrodes are modelled with tip *vs.* plane configurations. Fig. 4a shows the corresponding electron transmission spectra of the molecular junctions in enol and keto forms after structural optimization, see Fig. S12 for detailed information. It shows that no molecular orbital enters the bias window for either BPPD-enol or BPPD-keto molecular junctions, and it is the tail of the lowest unoccupied molecular orbital (LUMO) that dominates the conductance of the molecular junctions. The LUMO of the enol isomer is located closer to the bias window compared to the keto isomer, resulting in a higher conductance of the enol isomer. To evaluate the effect of electrode geometry, we performed additional transport calculations using two tip-shaped Au electrodes (Fig. S13), showing a conclusion consistent with that for the planar substrate. Additionally, the transmission pathways for electrons transporting from the left to the right electrode at E_F show that the reflection of electrons at the right electrode–molecule contact for the enol form is evidently smaller than that of the keto form (Fig. S14), which results in the larger conductance of the enol form and confirms our experimental observations. To further clarify the rectification behaviour of BPPD in the enol form, we carried out bias-dependent transport calculations (Fig. S15). The LUMO of BPPD in the keto form shifts symmetrically under both bias polarities. In contrast, the LUMO of BPPD in the enol form exhibits an asymmetry feature, leading to the rectification behaviour.

To provide a straightforward visualization, we further calculated the spatial distributions of the transmission eigenstates of the molecular junctions in the two forms, as shown in Fig. 4b. The transmission eigenstate of the enol form shows a more delocalized distribution, which evidently enters the right electrode. In contrast, the transmission eigenstate of the keto form shows a relatively localized distribution around the left electrode and the molecule backbone, and scarcely extends to the right electrode, leading to the low conductance of the keto form. With a close examination of the phase of the transmission eigenstate, we can obtain a deeper understanding of the transmission eigenstate distributions and the conductance of the two molecular junctions. It shows that, due to the existence of the hydrogen bond in the enol form, a 2π phase shift occurs for a small proportion of the transmission eigenstate at the right electrode–molecule contact of the molecular junction, which results in partial constructive interference of the transmission eigenstates and promotes the electron transport into the right electrode. However, for the keto form, the transmission eigenstate is superposed only by two states with a π phase difference at the right electrode–molecule contact. Therefore, destructive interference takes place at the right end of the molecule, hindering electrons from entering the right electrode and thus decreasing the conductance of the molecular junction. A more detailed analysis of the physical origin of this specific phase modulation can be found in Fig. S16.

To uncover the mechanism of the light-promoted enol–keto tautomerization observed in β-diketone derivative BPPD, the potential energy profile (PEB) was further calculated. As shown in Fig. 4c, the enol form is highly stable in its ground state E (S_0), with a high energy barrier (61.46 kcal mol^{-1}) for transformation to the keto tautomer. Upon 365 nm UV irradiation, the enol form is photoexcited to its first singlet excited state E^* (S_1) at 76.57 kcal mol^{-1} by adsorbing the photon energy. In this excited state, the intramolecular hydrogen bond is broken with the assistance of field-enhanced vibrations upon light absorption, enabling a facile proton transfer from the hydroxyl to the methyl group as marked by the red colour in BPPD structure through a transition state located at 102.72 kcal mol^{-1}. Despite the high absolute energy of the transition state, the activation barrier from E^* (S_1) is significantly reduced, allowing the system to evolve efficiently toward the excited-state keto form (K^* (S_1),

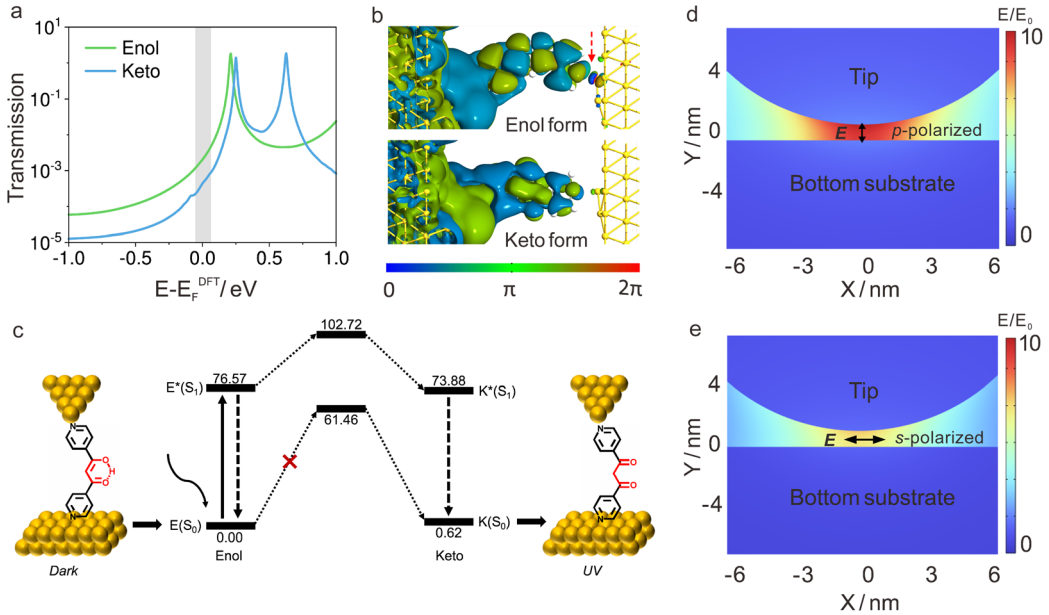

Fig. 4 Theoretical calculations of BPPD single-molecule junctions and the simulation of the optical field distribution upon light irradiation. (a) Transmission spectra of single molecular junctions with sandwiched BPPD in the enol form and keto form. The grey rectangle indicates the bias window of the molecular junctions. (b) The transmission eigenstates of BPPD molecular junctions in the enol form and keto form with optimized structures. The red dashed arrow indicates the point where the wavefunction with 0 phase (blue colour) overlaps with the wavefunction with 2π phase (red colour), resulting in constructive interference. (c) Potential energy profile for the photoinduced enol–keto tautomerization of BPPD *via* intramolecular proton transfer in TCB solution. (d) Spatial distribution of the electric field enhancement factor (E/E_0) in the nanogap upon p-polarized light and (e) upon s-polarized light (365 nm) irradiation.

73.88 kcal mol^{-1}). Subsequent internal conversion brings the system down to the ground-state keto tautomer (K (S_0), 0.62 kcal mol^{-1}). These results demonstrate that UV light is essential for enabling the enol → keto transformation *via* excited-state intramolecular proton transfer,[22] and that the product is effectively trapped in the keto form due to an energetically asymmetric pathway.

It has been extensively reported that a localized surface plasmon is generated and the optical field is greatly enhanced within the nanogap upon light irradiation.[11,52,53] To evaluate the plasmon-mediated mechanism, we performed numerical simulations of the electromagnetic field intensity in the nanogap using the finite element method (FEM), see SI methods for details. The junction was modelled with a planar gold electrode as the bottom electrode and a spherical gold electrode as the top electrode separated by 0.8 nm. Fig. 4d and f show the spatial field distributions upon p-polarized and s-polarized light illumination, respectively. Under p-polarized light, a pronounced field enhancement is observed at the centre of the gap, forming a localized plasmonic "hot spot" between the two electrodes even with a smoothed surface. Fig. 4d shows that the intensity of incident p-polarized light was greatly enhanced ($|E/E_0|^2 \sim 100$) in the nanogap between the two antenna electrodes, which would strongly excite the molecule and accelerate hydrogen bond breaking, promoting the localized enol → keto transformation.

Depending on the wavelength of incident light and the atomic-scale morphology of the electrode, we have demonstrated previously that the optical field can be enhanced by three orders of magnitude inside the nanocavity.[16,54] Therefore, the strongly enhanced optical field plays an important role in promoting the enol → keto transformation in addition to inducing changes in the energy landscape: (1) the strongly enhanced optical field increases photon absorption, leading to the enhancement of molecular vibrations, a mechanism similar to surface-enhanced Raman spectroscopy.[55] The enhanced vibrations in the nanogap facilitate the breaking of hydrogen bonds, thus promoting the enol → keto transformation; (2) the plasmon-induced vibration of the molecule breaks the hydron bond. It has been demonstrated that molecules adsorbed on metal surfaces can be dissociated by the optically excited plasmon at the STM–BJ junction.[56] The dissociation of the molecule can be realized *via* either the direct intramolecular excitation of electrons from the HOMO to the LUMO through the decay of the optically excited LSP in the nanogap[56] or the indirect transfer of hot electrons from the electrode to the molecule, accompanied by vibrational excitation.[57] Similarly, the hydrogen bonds with weak bond energy are highly likely to be broken by the plasmon-induced vibrations, thereby lowering the barrier for proton transfer and promoting enol-to-keto transformation within the confined and enhanced optical field.

Conclusions

We explored the keto–enol tautomerism of β-diketone derivatives (BPPD). Utilizing *in situ* conductance measurements of thousands of single-molecule junctions, optical spectroscopy, and flicker noise analysis, we demonstrated that BPPD in the

enol form can be transformed to the keto form upon ultralow power UV irradiation using antenna electrodes. Assisted by FEM-based simulations, it is revealed that the intensity of incident p-polarized light is greatly enhanced in the nanogap between the two antenna electrodes, which makes it feasible to trigger the localized enol → keto transformation by accelerating hydrogen bond breaking and intramolecular proton transfer upon light irradiation. Correspondingly, we revealed that the conductance of BPPD in the enol form is one order of magnitude higher than in the keto form, and the enol form presents a rectifying feature which is completely absent in the keto form, even though both have the same anchoring group and identical length, thereby demonstrating that the intramolecular hydron bond plays a critical role in determining electron transport. Our study clarified the mechanism for the confined optical field regulated enol–keto tautomerism, provided a strategy to distinguish the two forms at the single-molecule level, and offered a potential approach to manipulate the enol–keto tautomerism one by one beyond chemical stimulations.

Author contributions

D. X., initiated the project. A. A., performed electrical measurements. X. Z performed UV-vis measurements. H. F. performed numerical simulations of electromagnetic field strength in nanogaps. H. W. provided technical support for data processing. Y. G., Y. Y., C. W., L. C. and Z. L. performed DFT calculations. A. A. and D. X., wrote the manuscript with contributions from all authors.

Conflicts of interest

The authors declare no competing financial interests.

Data availability

Detailed experimental and computational data are provided in the SI. This includes the experimental procedures, conductance measurements, UV-vis spectral data, dipole moment calculations under external electric fields, electrostatic potential mapping, and 2D conductance histograms upon UV light exposure. Additional sections cover flicker noise analysis of BPPD junctions under irradiation, conductance characteristics of PY-3C, wavelength-dependent conductance behaviour, and transmission spectra and pathway analyses. All raw and processed data supporting these findings are available in the SI in tabulated or graphical form. Data files include original histograms, fitting curves, spectral analysis results, and calculated electronic structure information. Full methodological details are provided to facilitate reproducibility. See DOI: **https://doi.org/10.1039/d5sc06085k**.

Acknowledgements

We acknowledge the financial support from the National Key R&D Program of China (2021YFA1200103) and the National Natural Science Foundation of China (22273041, 12474286, 12174201), and the Natural Science Foundation of Tianjin (19JCZDJC31000, 19JCJQJC60900, 22JCYBJC01310).

Notes and references

1 E. D. Raczyńska, W. Kosińska, B. Ośmiałowski and R. Gawinecki, Tautomeric Equilibria in Relation to Pi-Electron Delocalization, *Chem. Rev.*, 2005, **105**, 3561–3612.
2 S. Radi, S. Tighadouini, O. Feron, O. Riant, M. Bouakka, R. Benabbes and Y. N. Mabkhot, Synthesis of Novel β-Keto-Enol Derivatives Tethered Pyrazole, Pyridine and Furan as New Potential Antifungal and Anti-Breast Cancer Agents, *Molecules*, 2015, **20**, 20186–20194.
3 D. R. Williams, J. C. Klein, L. C. Kopel, N. Nguyen and D. J. Tantillo, Studies toward Australifungin. A Synthesis Dilemma of Regioselective Keto–Enol Tautomerization, *Org. Lett.*, 2016, **18**, 424–427.
4 H. Gu, W. Wang, W. Wu, M. Wang, Y. Liu, Y. Jiao, F. Wang, F. Wang and X. Chen, Excited-state intramolecular proton transfer (ESIPT)-based fluorescent probes for biomarker detection: design, mechanism, and application, *Chem. Commun.*, 2023, **59**, 2056–2071.
5 F. Chu, G. Hai, D. Zhao, S. Liu, Y. Hu, G. Zhao, B. Peng, G. Wang and X. Huang, Regulating Keto–Enol Tautomerism of β-Ketoenamine Covalent–Organic Frameworks for Photocatalytic Oxidative Coupling of Amines, *ACS Catal.*, 2023, **13**, 13167–13180.
6 Z.-Q. Wang, M.-H. Li, S. Liang, Y. Kong, C. Wang, L. Li, J.-J. Xu and Y.-W. Yang, Regulating Enol-to-Keto Tautomerization of Pillararene-Based Conjugated Macrocycle Polymers for H2O2 Photosynthesis, *J. Am. Chem. Soc.*, 2025, **147**, 13618–13628.
7 L. Chen, P.-Y. Fu, H.-P. Wang and M. Pan, Excited-State Intramolecular Proton Transfer (ESIPT) for Optical Sensing in Solid State, *Adv. Opt. Mater.*, 2021, **9**, 2001952.
8 P. E. Hansen, Structural Studies of β-Diketones and Their Implications on Biological Effects, *Pharmaceuticals*, 2021, **14**, 1189.
9 C. Tang, T. Stuyver, T. Lu, J. Liu, Y. Ye, T. Gao, L. Lin, J. Zheng, W. Liu, J. Shi, S. Shaik, H. Xia and W. Hong, Voltage-driven control of single-molecule keto-enol equilibrium in a two-terminal junction system, *Nat. Commun.*, 2023, **14**, 3657.
10 H. Lu, H. Ye, M. Zhang, L. Wang and L. You, Photoswitchable Keto–Enol Tautomerism Driven by Light-Induced Change in Antiaromaticity, *Org. Lett.*, 2022, **24**, 8639–8644.
11 M. Wang, T. Wang, O. S. Ojambati, T. J. Duffin, K. Kang, T. Lee, E. Scheer, D. Xiang and C. A. Nijhuis, Plasmonic phenomena in molecular junctions: principles and applications, *Nat. Rev. Chem.*, 2022, **6**, 681–704.
12 J. B. Asbury, T. Steinel, C. Stromberg, K. J. Gaffney, I. R. Piletic and M. D. Fayer, Hydrogen bond breaking probed with multidimensional stimulated vibrational echo correlation spectroscopy, *J. Chem. Phys.*, 2003, **119**, 12981–12997.

13 B. Xu and N. J. Tao, Measurement of Single-Molecule Resistance by Repeated Formation of Molecular Junctions, *Science*, 2003, **301**, 1221–1223.
14 X. Zhao, Y. Yan, M. Tan, S. Zhang, X. Xu, Z. Zhao, M. Wang, X. Zhang, A. Adijiang, Z. Li, E. Scheer and D. Xiang, Molecular dimer junctions forming: Role of disulfide bonds and electrode-compression-time, *SmartMat*, 2024, **146**(10), e1280.
15 M. Tan, F. Sun, X. Zhao, Z. Zhao, S. Zhang, X. Xu, A. Adijiang, W. Zhang, H. Wang, C. Wang, Z. Li, E. Scheer and D. Xiang, Conductance Evolution of Photoisomeric Single-Molecule Junctions under Ultraviolet Irradiation and Mechanical Stretching, *J. Am. Chem. Soc.*, 2024, **146**, 6856–6865.
16 W. Zhang, H. Liu, J. Lu, L. Ni, H. Liu, Q. Li, M. Qiu, B. Xu, T. Lee, Z. Zhao, X. Wang, M. Wang, T. Wang, A. Offenhäusser, D. Mayer, W.-T. Hwang and D. Xiang, Atomic switches of metallic point contacts by plasmonic heating, *Light Sci. Appl.*, 2019, **8**, 34.
17 O. Coddington, J. L. Lean, P. Pilewskie, M. Snow and D. Lindholm, A Solar Irradiance Climate Data Record, *Bull. Am. Meteorol. Soc.*, 2016, **97**, 1265–1282.
18 W. Wang and L. Yu, Intramolecular Hydrogen Bonding Assisted Charge Transport through Single Rectifying Molecule, *Langmuir*, 2011, **27**, 2084–2087.
19 T. Nishino, N. Hayashi and P. T. Bui, Direct Measurement of Electron Transfer through a Hydrogen Bond between Single Molecules, *J. Am. Chem. Soc.*, 2013, **135**, 4592–4595.
20 L. Ge, S. Hou, Y. Chen, Q. Wu, L. Long, X. Yang, Y. Ji, L. Lin, G. Xue, J. Liu, X. Liu, C. J. Lambert, W. Hong and Y. Zheng, Hydrogen-bond-induced quantum interference in single-molecule junctions of regioisomers, *Chem. Sci.*, 2022, **13**, 9552–9559.
21 X. Xie, P. Li, Y. Xu, L. Zhou, Y. Yan, L. Xie, C. Jia and X. Guo, Single-Molecule Junction: A Reliable Platform for Monitoring Molecular Physical and Chemical Processes, *ACS Nano*, 2022, **16**, 3476–3505.
22 X. Wang, H. Chen, Y. Lei, Y. Li and B. Xiao, Photoconductance Induced by Excited-State Intramolecular Proton Transfer (ESIPT) in Single-Molecule Junctions, *Adv. Mater.*, 2024, **36**, 2413529.
23 D. Dulić, S. J. van der Molen, T. Kudernac, H. T. Jonkman, J. J. D. de Jong, T. N. Bowden, J. van Esch, B. L. Feringa and B. J. van Wees, One-Way Optoelectronic Switching of Photochromic Molecules on Gold, *Phys. Rev. Lett.*, 2003, **91**, 207402.
24 C. Jia, A. Migliore, N. Xin, S. Huang, J. Wang, Q. Yang, S. Wang, H. Chen, D. Wang, B. Feng, Z. Liu, G. Zhang, D.-H. Qu, H. Tian, M. A. Ratner, H. Q. Xu, A. Nitzan and X. Guo, Covalently bonded single-molecule junctions with stable and reversible photoswitched conductivity, *Science*, 2016, **352**, 1443–1445.
25 X. Xu, C. Gao, R. Emusani, C. Jia and D. Xiang, Toward Practical Single-Molecule/Atom Switches, *Adv. Sci.*, 2024, **11**, 2400877.
26 Y. Chen, H.-C. Wang, Y. Tang, Y. Zhou, L. Huang, J. Cao, C. Tang, M. Zhang, J. Shi, J. Liu, X. Ren, Y.-X. Xu and W. Hong, Modulation of charge transport through single-molecule bilactam junctions by tuning hydrogen bonds, *Chem. Commun.*, 2021, **57**, 1935–1938.
27 J.-H. Fang, Z.-H. Zhao, A.-X. Li and L. Wang, Electron Transport through Hydrogen Bonded Single-Molecule Junctions, *Chin. J. Chem.*, 2023, **41**, 3433–3446.
28 A. I. Yanson, G. R. Bollinger, H. E. van den Brom, N. Agraït and J. M. van Ruitenbeek, Formation and manipulation of a metallic wire of single gold atoms, *Nature*, 1998, **395**, 783–785.
29 W. Hong, D. Z. Manrique, P. Moreno-García, M. Gulcur, A. Mishchenko, C. J. Lambert, M. R. Bryce and T. Wandlowski, Single Molecular Conductance of Tolanes: Experimental and Theoretical Study on the Junction Evolution Dependent on the Anchoring Group, *J. Am. Chem. Soc.*, 2012, **134**, 2292–2304.
30 P. Markov and I. Petkov, On the photosensitivity of dibenzoylmethane, benzoylacetone and ethyl benzoylacetate in solution, *Tetrahedron*, 1977, **33**, 1013–1015.
31 L. Venkataraman, J. E. Klare, C. Nuckolls, M. S. Hybertsen and M. L. Steigerwald, Dependence of single-molecule junction conductance on molecular conformation, *Nature*, 2006, **442**, 904–907.
32 H. Zhang, W. Xu, K. Song, T. Lu, G. Zhang, Y. Zang, W. Hong and D. Zhang, Dual Modulation of Single Molecule Conductance via Tuning Side Chains and Electric Field with Conjugated Molecules Entailing Intramolecular O···S Interactions, *Adv. Sci.*, 2022, **9**, 2105667.
33 Z. Wang, M. Huang, J. Dong, X. Wang, Y. Li, M. Sun and S. Chang, Utilizing Noncovalent Conformational Locks to Create Through-Space Charge Transport, *J. Phys. Chem. C*, 2023, **127**, 2518–2523.
34 G. R. Berdiyorov, Influence of pyridinic nitrogen on tautomeric shifts and charge transport in single molecule keto enol equilibria, *Sci. Rep.*, 2025, **15**, 3018.
35 A. Mishchenko, D. Vonlanthen, V. Meded, M. Bürkle, C. Li, I. V. Pobelov, A. Bagrets, J. K. Viljas, F. Pauly, F. Evers, M. Mayor and T. Wandlowski, Influence of Conformation on Conductance of Biphenyl-Dithiol Single-Molecule Contacts, *Nano Lett.*, 2010, **10**, 156–163.
36 O. Adak, E. Rosenthal, J. Meisner, E. F. Andrade, A. N. Pasupathy, C. Nuckolls, M. S. Hybertsen and L. Venkataraman, Flicker Noise as a Probe of Electronic Interaction at Metal–Single Molecule Interfaces, *Nano Lett.*, 2015, **15**, 4143–4149.
37 M. H. Garner, H. Li, Y. Chen, T. A. Su, Z. Shangguan, D. W. Paley, T. Liu, F. Ng, H. Li, S. Xiao, C. Nuckolls, L. Venkataraman and G. C. Solomon, Comprehensive suppression of single-molecule conductance using destructive σ-interference, *Nature*, 2018, **558**, 415–419.
38 Y. Tang, Y. Zhou, D. Zhou, Y. Chen, Z. Xiao, J. Shi, J. Liu and W. Hong, Electric Field-Induced Assembly in Single-Stacking Terphenyl Junctions, *J. Am. Chem. Soc.*, 2020, **142**, 19101–19109.
39 W. Zhang, Z. Zhao, M. Tan, A. Adijiang, S. Zhong, X. Xu, T. Zhao, E. Ramya, L. Sun, X. Zhao, Z. Fan and D. Xiang, Regulating the orientation of a single coordinate bond by

the synergistic action of mechanical forces and electric field, *Chem. Sci.*, 2023, **14**, 11456–11465.

40 I. Díez-Pérez, J. Hihath, Y. Lee, L. Yu, L. Adamska, M. A. Kozhushner, I. I. Oleynik and N. Tao, Rectification and stability of a single molecular diode with controlled orientation, *Nat. Chem.*, 2009, **1**, 635–641.

41 J. Hihath, C. Bruot, H. Nakamura, Y. Asai, I. Díez-Pérez, Y. Lee, L. Yu and N. Tao, Inelastic Transport and Low-Bias Rectification in a Single-Molecule Diode, *ACS Nano*, 2011, **5**, 8331–8339.

42 R. Gupta, J. A. Fereiro, A. Bayat, A. Pritam, M. Zharnikov and P. C. Mondal, Nanoscale molecular rectifiers, *Nat. Rev. Chem.*, 2023, **7**, 106–122.

43 G. M. Morales, P. Jiang, S. Yuan, Y. Lee, A. Sanchez, W. You and L. Yu, Inversion of the Rectifying Effect in Diblock Molecular Diodes by Protonation, *J. Am. Chem. Soc.*, 2005, **127**, 10456–10457.

44 W.-B. Cai, L.-J. Wan, H. Noda, Y. Hibino, K. Ataka and M. Osawa, Orientational Phase Transition in a Pyridine Adlayer on Gold(111) in Aqueous Solution Studied by in situ Infrared Spectroscopy and Scanning Tunneling Microscopy, *Langmuir*, 1998, **14**, 6992–6998.

45 T. Chen, P.-X. Dai, J.-Y. Wu, D. Wang and L.-J. Wan, Disorder–Order Transformation of Trithiocyanuric Acid Adlayer on a Au(111) Surface Induced by Electrode Potential, *J. Phys. Chem. C*, 2011, **115**, 16583–16589.

46 Q.-N. Zheng, X.-H. Liu, T. Chen, H.-J. Yan, T. Cook, D. Wang, P. J. Stang and L.-J. Wan, Formation of Halogen Bond-Based 2D Supramolecular Assemblies by Electric Manipulation, *J. Am. Chem. Soc.*, 2015, **137**, 6128–6131.

47 W. Sauerbier, Effects of Ultra-Violet Light on Hydrogen Bonds in Deoxyribonucleic Acid of Phage T1, *Nature*, 1960, **188**, 329–330.

48 Z. Yu, Y. X. Xu, J. Q. Su, P. M. Radjenovic, Y. H. Wang, J. F. Zheng, B. Teng, Y. Shao, X. S. Zhou and J. F. Li, Probing Interfacial Electronic Effects on Single-Molecule Adsorption Geometry and Electron Transport at Atomically Flat Surfaces, *Angew. Chem., Int. Ed.*, 2021, **60**, 15452.

49 J. Taylor, H. Guo and J. Wang, Ab initio modeling of quantum transport properties of molecular electronic devices, *Phys. Rev. B*, 2001, **63**, 245407.

50 M. Brandbyge, J.-L. Mozos, P. Ordejón, J. Taylor and K. Stokbro, Density-functional method for nonequilibrium electron transport, *Phys. Rev. B*, 2002, **65**, 165401.

51 F. Sun, L. Liu, C.-F. Zheng, Y.-C. Li, Y. Yan, X.-X. Fu, C.-K. Wang, R. Liu, B. Xu and Z.-L. Li, Decoding the mechanical conductance switching behaviors of dipyridyl molecular junctions, *Nanoscale*, 2023, **15**, 12586–12597.

52 M. Wang, J. Zhang, A. Adijiang, X. Zhao, M. Tan, X. Xu, S. Zhang, W. Zhang, X. Zhang, H. Wang and D. Xiang, Plasmon-Assisted Trapping of Single Molecules in Nanogap, *Materials*, 2023, **16**, 3230.

53 C. Zhan, G. Wang, J. Yi, J.-Y. Wei, Z.-H. Li, Z.-B. Chen, J. Shi, Y. Yang, W. Hong and Z.-Q. Tian, Single-Molecule Plasmonic Optical Trapping, *Matter*, 2020, **3**, 1350–1360.

54 X. Xu, Q. Qi, Q. Hu, L. Ma, R. Emusani, S. Zhang, X. Zhao, M. Tan, A. Adijiang, W. Zhang, Z. Ma, G. Tian, E. Scheer and D. Xiang, Manipulating π–π Interactions between Single Molecules by Using Antenna Electrodes as Optical Tweezers, *Phys. Rev. Lett.*, 2024, **133**, 233001.

55 S. Schlücker, Surface-Enhanced Raman Spectroscopy: Concepts and Chemical Applications, *Angew. Chem., Int. Ed.*, 2014, **53**, 4756–4795.

56 E. Kazuma, J. Jung, H. Ueba, M. Trenary and Y. Kim, Real-space and real-time observation of a plasmon-induced chemical reaction of a single molecule, *Science*, 2018, **360**, 521–526.

57 P. Christopher, H. Xin and S. Linic, Visible-light-enhanced catalytic oxidation reactions on plasmonic silver nanostructures, *Nat. Chem.*, 2011, **3**, 467–472.